Modeling and Control of Power-Split Hybrid Electric Vehicles

Roberto Zanasi
Information Engineering Department
University of Modena e Reggio Emilia
Via Vignolese 905
41100 Modena, Italy
roberto.zanasi@unimore.it

Federica Grossi
Information Engineering Department
University of Modena e Reggio Emilia
Via Vignolese 905
41100 Modena, Italy
federica.grossi@unimore.it

***Abstract*—In this paper a Power-split hybrid automotive system is considered, including a multi-phase synchronous motor, an internal combustion engine and a planetary gear as key element to split power in this propulsion system. The dynamic model of a planetary gear with internal elasticity is presented and the model of the whole vehicle is given using the Power-Oriented Graphs approach. A global control is designed to obtain different operation modes of the vehicle: engine start, battery charging, hybrid traction, recovery of braking energy. Simulation results of the modeled HEV are provided showing the effectiveness of the proposed model and control.**

I. Introduction

The analysis of the dynamic behavior of hybrid electric vehicles is nowadays a very important topic, especially aiming at reducing fuel consumption and exhaust emissions. The definition of hybrid vehicle comes from the presence on the vehicle of two different energy sources. This paper deals with power-split propulsion system of hybrid electric vehicles, in particular the one equipped with an internal combustion engine and one electric machine with batteries and where the power split is carried out by means of a planetary gear system. In this paper the Power-Oriented Graphs (POG) modeling technique is exploited to provide the models of the considered dynamic systems: a planetary gear with internal elasticity and dissipation, a multi-phase permanent magnet synchronous motor and a power-split hybrid vehicle. The POG technique allows to graphically describe the dynamic model of any type of physical system (in different energetic domains) putting in evidence the power flows within the modeled systems. The POG schemes are easy to use, easy to understand even by a neophyte and can be directly implemented in Simulink. Starting from the analysis of the power flows the control of the vehicle propulsion is designed. Different operation modes are possible and they will be examined in the paper. The paper is organized as follows: Sec. II states the POG basic features, Sec. III introduces the HEV model and Sec. IV shows simulation results.

II. Power-Oriented Graphs basic features

The Power-Oriented Graphs technique, see [1], is suitable for modeling physical systems. The POG block schemes are normal block diagrams combined with a particular modular structure essentially based on the use of the two blocks shown in Fig. 1.a and Fig. 1.b: the *elaboration block* (e.b.) stores and/or dissipates energy (i.e. springs, masses, dampers, capacities, inductances, resistances, etc.); the *connection block* (c.b.) redistributes the power within the system without storing nor dissipating energy (i.e. gear reduction, transformers, etc.). The e.b. and the c.b. are suitable for representing both scalar and vectorial systems. In the vectorial case, $\mathbf{G}(s)$ and $\mathbf{K}$ are matrices: $\mathbf{G}(s)$ is always a square matrix composed by positive real transfer functions; matrix $\mathbf{K}$ can also be rectangular. The circle present in the e.b. is a summation element and the black spot represents a minus sign that multiplies the entering variable. Power-Oriented Graphs keep a direct correspondence between the dashed sections of the graphs and real power sections of the modeled systems: the scalar product $\mathbf{x}^{\mathrm{T}}\mathbf{y}$ of the two *power vectors* $\mathbf{x}$ and $\mathbf{y}$ involved in each dashed line of a power-oriented graph, see Fig. 1, has the physical meaning of *power flowing through that particular section*. The Bond Graphs technique, see [2] and [3], is based on the same idea, but it uses a different and specific graphical representation.

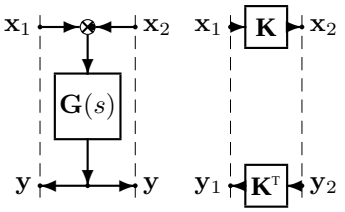

a) *e. b.* b) *c. b.*

	POG Variables	
Domains:	*Across:* v_e	*Through:* v_f
Electrical	Voltage V	Current I
Mec. Tra.	Velocity v	Force F
Mec. Rot.	Ang. Vel. ω	Torque τ
Hydraulic	Pressure P	Flow rate Q

c) *Across and through variables*

Figure 1. POG basic blocks and variables: a) *elaboration block*; b) *connection block*; c) *across and through variables*.

The main energetic domains encountered in modeling physical systems are the electrical, the mechanical (translational and rotational) and the hydraulic, see Fig. 1.c. Each energetic domain is characterized by two *power variables*: an *across-variable* v_e defined between two points (i.e. the voltage V, the velocity $\dot{x}$, etc.), and a *through-variable* v_f defined in each point of the space (i.e. the current I, the force F, etc.). Each Physical Element (PE) interacts with the external world through the power sections associated to its terminals.

978-1-4244-8218-4/10/$26.00 ©2010 IEEE

Another important property of the POG technique is the direct correspondence between the POG schemes and the corresponding state space dynamic equations. For example, the POG scheme shown in Fig. 2 can be represented by the state space equations (1) where the *energy matrix* $\mathbf{L}$ is symmetric and positive definite: $\mathbf{L} = \mathbf{L}^{\mathrm{T}} > 0$. It can be easily shown that when $\mathbf{D} = 0$ it follows that $\mathbf{C} = \mathbf{B}^{\mathrm{T}}$.

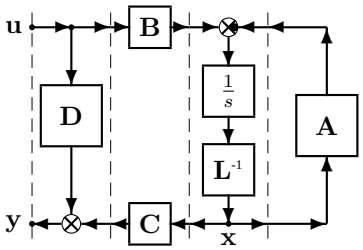

$$\begin{cases} \mathbf{L}\,\dot{\mathbf{x}} = -\mathbf{A}\,\mathbf{x} + \mathbf{B}\,\mathbf{u} \\ \mathbf{y} = \mathbf{C}\,\mathbf{x} + \mathbf{D}\,\mathbf{u} \end{cases} \quad (1)$$

$$\Downarrow (\mathbf{x} = \mathbf{T}\,\mathbf{z})$$

$$\begin{cases} \overline{\mathbf{L}}\,\dot{\mathbf{z}} = -\overline{\mathbf{A}}\,\mathbf{z} + \overline{\mathbf{B}}\,\mathbf{u} \\ \mathbf{y} = \overline{\mathbf{C}}\,\mathbf{z} + \overline{\mathbf{D}}\,\mathbf{u} \end{cases} \quad (2)$$

Figure 2. POG block scheme of a generic dynamic system.

III. POG MODELING OF AN HYBRID AUTOMOTIVE SYSTEM

The power-split architecture considered in this paper is shown in Fig. 3: it includes an internal combustion engine (ICE), a multi-phase Permanent Magnet Synchronous Machine (PMSM) and the vehicle, see [4], [10] for other architectures. The ICE is rigidly connected to the Carrier (C), the PMSM is connected to the Sun (S) and the vehicle driving axle is connected to the Ring (R). This hybrid system can be dynamically described by the "high level" POG block scheme shown in Fig. 4. Note that the power sections ①-⑤ shown in Fig. 4 correspond to the physical power sections indicated in Fig. 3.

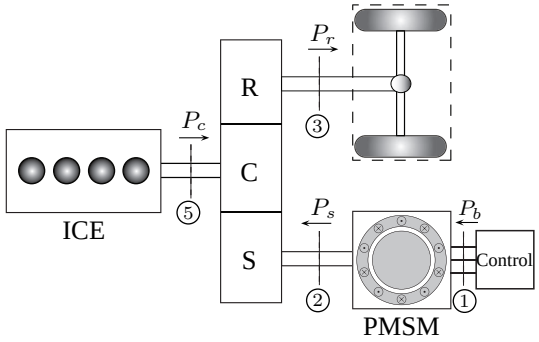

Figure 3. Scheme of the considered power structure of the vehicle

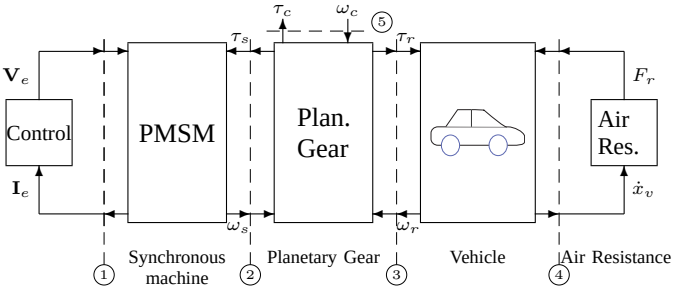

Figure 4. POG graphical representation of the considered hybrid vehicle.

Hybrid propulsion systems also include some devices in order to store electrical energy such as batteries, supercapacitors and others, but in this paper they are not taken into account.

A. Internal Combustion Engine model

In order to simulate the hybrid power train an engine model is needed. Since for our focus it is sufficient to consider the main mechanical dynamics of the engine, a simplified model is proposed. In Fig. 5 the POG scheme of the proposed engine model is shown, where J_e is the engine shaft inertia, b_e is the friction coefficient and $\omega_{c_{ref}}$ is the reference rotational velocity. The throttle control is a proportional controller K_{ice}

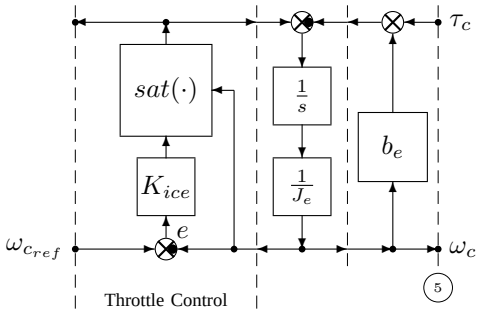

Figure 5. POG scheme of the ICE model.

with a saturation $sat(\cdot) = sat\left(K_{ice}e, \tau(\omega_c)\right)$. The saturation depends on ω_c according to the ICE torque-speed map reported in Fig.6.

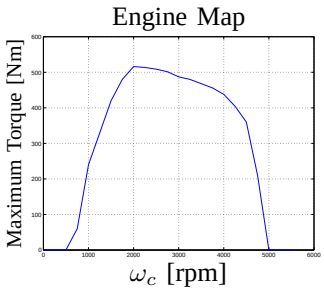

Figure 6. Internal combustion engine Torque−Speed map.

B. Planetary Gear modeling

Let us consider the planetary gear shown in Fig. 7. The main parameters of the system are: r_s, r_c, r_r and r_p are the sun, carrier, ring and planet radii; J_s, b_s, J_c, b_c, J_r, b_r, J_p and b_p are the inertia and linear friction coefficients of the sun, carrier ring and planet, respectively; K_{sc}, d_{sc}, K_{cr} and d_{cr} are the stiffness and friction coefficients of the sun-carrier and carrier-ring elastic elements, respectively.

The carrier, the planets and the ring interact each other through the two elastic elements K_{cr} and K_{sc}. Considering that the planetary gear inertias will be connected to the shafts of the ICE, PMSM and driving axle of the vehicle, it is convenient to provide a reduced elastic model of the planetary gear when inertias J_s, J_c and J_r go to zero. In [7] the POG technique is exploited to obtain different reduced models of the planetary gear using proper mathematical transformations.

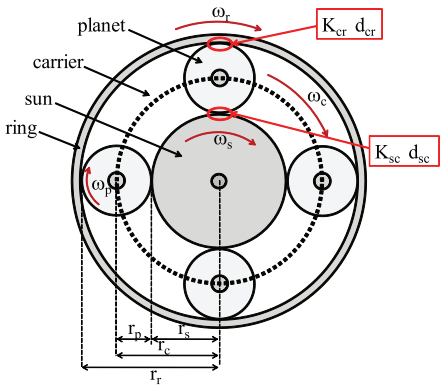

Figure 7. Planetary gear and related parameters.

m_s	number of motor phases;
p	number of polar expansions;
θ, θ_m	electric and rotor angular positions: $\theta = p\,\theta_m$;
ω, ω_m	electric and rotor angular velocities: $\omega = p\,\omega_m$;
R_s	i-th stator phase resistance;
L_s	i-th stator phase self induction coefficient;
M_{s0}	maximum value of mutual inductance between stator phases;
$\phi_c(\theta)$	total rotor flux chained with stator phase 1;
φ_c	maximum value of function $\phi_c(\theta)$;
J_m	rotor moment of inertia;
b_m	rotor linear friction coefficient;
τ_m	electromotive torque acting on the rotor;
τ_e	external load torque acting on the rotor;
γ_s	basic angular displacement ($\gamma_s = 2\pi/m_s$)

Table I
PARAMETERS OF THE MULTI-PHASE SYNCHRONOUS MOTOR.

The state space equations of the system are shown in Fig. 8 and in compact form they can be written as

$$\begin{cases} \tilde{\mathbf{L}}_e\,\dot{\tilde{\mathbf{x}}} &= -\tilde{\mathbf{A}}_e\,\tilde{\mathbf{x}} + \tilde{\mathbf{B}}_e\,\tilde{\mathbf{u}} \\ \tilde{\mathbf{y}} &= \tilde{\mathbf{C}}_e\,\tilde{\mathbf{x}} + \tilde{\mathbf{D}}_e\,\tilde{\mathbf{u}} \end{cases} \tag{3}$$

Note that in this elastic model the velocities are the input and the torques are the output.

C. Electrical motors modeling

In this paper we refer to a permanent magnet synchronous motor with an *odd* number m_s of star-connected phases [6] characterized by the parameters shown in Tab. I. Let us introduce the following vectors:

$${}^t\mathbf{I}_s = \begin{bmatrix} I_{s1} \\ I_{s2} \\ \vdots \\ I_{sm_s} \end{bmatrix},\quad {}^t\mathbf{V}_s = \begin{bmatrix} V_{s1} \\ V_{s2} \\ \vdots \\ V_{sm_s} \end{bmatrix},\quad {}^t\dot{\mathbf{q}} = \begin{bmatrix} {}^t\mathbf{I}_s \\ \omega_m \end{bmatrix},\quad {}^t\mathbf{V} = \begin{bmatrix} {}^t\mathbf{V}_s \\ -\tau_s \end{bmatrix} \tag{5}$$

where ${}^t\mathbf{I}_s$, ${}^t\mathbf{V}_s$ are the current and voltage stator vectors and ${}^t\dot{\mathbf{q}}$, ${}^t\mathbf{V}$ are the state and input vectors of the global system. Using a "Lagrangian" approach, see [5], the dynamic equations of the electric motor are obtained:

$$\underbrace{\left[\begin{array}{c|c} {}^t\mathbf{L}_s & 0 \\ \hline 0 & J_m \end{array}\right]}_{{}^t\mathbf{L}} \underbrace{\begin{bmatrix} {}^t\dot{\mathbf{I}}_s \\ \dot{\omega}_m \end{bmatrix}}_{{}^t\ddot{\mathbf{q}}} = -\underbrace{\left[\begin{array}{c|c} {}^t\mathbf{R}_s & {}^t\mathbf{K}_\tau(\theta) \\ \hline -{}^t\mathbf{K}_\tau^{\mathrm{T}}(\theta) & b_m \end{array}\right]}_{{}^t\mathbf{R}\,+\,{}^t\mathbf{W}} \underbrace{\begin{bmatrix} {}^t\mathbf{I}_s \\ \omega_m \end{bmatrix}}_{{}^t\dot{\mathbf{q}}} + \underbrace{\begin{bmatrix} {}^t\mathbf{V}_s \\ -\tau_s \end{bmatrix}}_{{}^t\mathbf{V}} \tag{6}$$

where matrix ${}^t\mathbf{L}_s$ is defined as follows:

$${}^t\mathbf{L}_s = L_{s0}\,\mathbf{I}_{m_s} + M_{s0} \overset{i}{\underset{1:m_s}{[\![}} \cos((i-j)\gamma_s) \overset{j}{\underset{1:m_s}{]\!]}}$$

with $L_{s0} = L_s - M_{s0}$. Matrices ${}^t\mathbf{R}$ and ${}^t\mathbf{W}$ are defined as:

$${}^t\mathbf{R} = \left[\begin{array}{c|c} {}^t\mathbf{R}_s & 0 \\ \hline 0 & b_m \end{array}\right],\qquad {}^t\mathbf{W} = \left[\begin{array}{c|c} 0 & {}^t\mathbf{K}_\tau(\theta) \\ \hline -{}^t\mathbf{K}_\tau^{\mathrm{T}}(\theta) & 0 \end{array}\right]$$

where ${}^t\mathbf{R}_s = R_s\,\mathbf{I}_{m_s}$ and the torque vector ${}^t\mathbf{K}_\tau(\theta)$ is:

$${}^t\mathbf{K}_\tau(\theta) = p\,\varphi_c \left\| \left[-\sum_{n=1:2}^{\infty} n\,a_n \sin[n(\theta - h\,\gamma_s)] \right] \right\|_{0:m_s-1}^{h}. \tag{7}$$

Parameters a_n in (7) are the coefficients of the periodic normalized rotor flux function $\bar{\phi}(\theta)$ expressed in Fourier series: $\bar{\phi}(\theta) = \sum_{n=1:2}^{\infty} a_n \cos(n\theta)$.

Let us now consider the transformation matrix:

$${}^\omega\mathbf{T}_t(\theta) = \sqrt{\frac{2}{m_s}} \left\| \begin{bmatrix} \cos(k\,(\theta - h\,\gamma_s)) \\ \sin(k\,(\theta - h\,\gamma_s)) \end{bmatrix} \right\|_{1:2:m_s-2}^{k}{}_{0:m_s-1}^{h} \tag{8}$$

which is a function of the electrical angle θ and transforms the system variables from the original reference frame Σ_t to a transformed rotating frame Σ_ω. Applying transformation ${}^t\dot{\mathbf{q}} = {}^\omega\mathbf{T}_t^{\mathrm{T}}\,{}^\omega\dot{\mathbf{q}}$ to system (6), one obtains the following transformed system:

$$\underbrace{\left[\begin{array}{c|c} {}^\omega\mathbf{L}_s & 0 \\ \hline 0 & J_m \end{array}\right]}_{{}^\omega\mathbf{L}} \underbrace{\begin{bmatrix} {}^\omega\dot{\mathbf{I}}_s \\ \dot{\omega}_m \end{bmatrix}}_{{}^\omega\ddot{\mathbf{q}}} = -\underbrace{\left[\begin{array}{c|c} {}^\omega\mathbf{R}_s + {}^\omega\mathbf{L}_s\,{}^\omega\mathbf{J}_s & {}^\omega\mathbf{K}_\tau(\theta) \\ \hline -{}^\omega\mathbf{K}_\tau^{\mathrm{T}}(\theta) & b_m \end{array}\right]}_{{}^\omega\mathbf{R}\,+\,{}^\omega\mathbf{W}} \underbrace{\begin{bmatrix} {}^\omega\mathbf{I}_s \\ \omega_m \end{bmatrix}}_{{}^\omega\dot{\mathbf{q}}} + \underbrace{\begin{bmatrix} {}^\omega\mathbf{V}_s \\ -\tau_s \end{bmatrix}}_{{}^\omega\mathbf{V}} \tag{9}$$

where ${}^\omega\mathbf{I}_s = {}^t\mathbf{T}_\omega^{\mathrm{T}}\,{}^t\mathbf{I}_s$, ${}^\omega\mathbf{L}_s = {}^t\mathbf{T}_\omega^{\mathrm{T}}\,{}^t\mathbf{L}_s\,{}^t\mathbf{T}_\omega$, ${}^\omega\mathbf{R}_s = {}^t\mathbf{T}_\omega^{\mathrm{T}}\,{}^t\mathbf{R}_s\,{}^t\mathbf{T}_\omega$, ${}^\omega\mathbf{J}_s = {}^t\mathbf{T}_\omega^{\mathrm{T}}\,{}^t\dot{\mathbf{T}}_\omega$, ${}^\omega\mathbf{K}_\tau = {}^t\mathbf{T}_\omega^{\mathrm{T}}\,{}^t\mathbf{K}_\tau$ e ${}^\omega\mathbf{V}_s = {}^t\mathbf{T}_\omega^{\mathrm{T}}\,{}^t\mathbf{V}_s$. Matrices ${}^\omega\mathbf{L}_s$ and ${}^\omega\mathbf{J}_s$ have the following structure:

$${}^\omega\mathbf{L}_s = \begin{bmatrix} L_{se} & 0 & 0 & \cdots & 0 \\ 0 & L_{se} & 0 & \cdots & 0 \\ 0 & 0 & L_{s0} & \cdots & 0 \\ \vdots & \vdots & \vdots & \ddots & \vdots \\ 0 & 0 & 0 & \cdots & L_{s0} \end{bmatrix},\quad {}^\omega\mathbf{J}_s = \left\| \begin{bmatrix} 0 & -k\,\omega \\ k\,\omega & 0 \end{bmatrix} \right\|_{1:2:m_s-2}^{k},$$

where $L_{se} = L_{s0} + \frac{m_s}{2} M_{s0}$ and $\omega = \dot{\theta}$. Vectors ${}^\omega\mathbf{I}_s$ and ${}^\omega\mathbf{V}_s$ in (9) are:

$${}^\omega\mathbf{I}_s = \left\| \left[{}^\omega\mathbf{I}_{sk} \right] \right\|_{1:2:m_s-2}^{k} = \left\| \begin{bmatrix} I_{dk} \\ I_{qk} \end{bmatrix} \right\|_{1:2:m_s-2}^{k},\qquad {}^\omega\mathbf{V}_s = \left\| \left[{}^\omega\mathbf{V}_{sk} \right] \right\|_{1:2:m_s-2}^{k} = \left\| \begin{bmatrix} V_{dk} \\ V_{qk} \end{bmatrix} \right\|_{1:2:m_s-2}^{k}$$

$$\underbrace{\begin{bmatrix} \frac{1}{K_{sc}} & 0 & 0 \\ 0 & J_p & 0 \\ 0 & 0 & \frac{1}{K_{cr}} \end{bmatrix}}_{\tilde{\mathbf{L}}_e} \underbrace{\begin{bmatrix} \dot{F}_{sc} \\ \dot{\omega}_p \\ \dot{F}_{cr} \end{bmatrix}}_{\dot{\tilde{\mathbf{x}}}} = \underbrace{\begin{bmatrix} 0 & r_p & 0 \\ -r_p & -r_p^2 d_{sc} - b_p - r_p^2 d_{cr} & -r_p \\ 0 & r_p & 0 \end{bmatrix}}_{-\tilde{\mathbf{A}}_e} \underbrace{\begin{bmatrix} F_{sc} \\ \omega_p \\ F_{cr} \end{bmatrix}}_{\tilde{\mathbf{x}}} + \underbrace{\begin{bmatrix} r_s & -r_s & 0 \\ -r_s d_{sc} r_p & r_s d_{sc} r_p - r_r d_{cr} r_p & r_r d_{cr} r_p \\ 0 & r_r & -r_r \end{bmatrix}}_{\tilde{\mathbf{B}}_e} \underbrace{\begin{bmatrix} \omega_s \\ \omega_c \\ \omega_r \end{bmatrix}}_{\tilde{\mathbf{u}}}$$

$$\underbrace{\begin{bmatrix} \tau_s \\ \tau_c \\ \tau_r \end{bmatrix}}_{\tilde{\mathbf{y}}} = \underbrace{\begin{bmatrix} r_s & r_s d_{sc} r_p & 0 \\ -r_s & -r_s d_{sc} r_p + r_r d_{cr} r_p & r_r \\ 0 & -r_r d_{cr} r_p & -r_r \end{bmatrix}}_{\tilde{\mathbf{C}}_e} \underbrace{\begin{bmatrix} F_{sc} \\ \omega_p \\ F_{cr} \end{bmatrix}}_{\tilde{\mathbf{x}}} + \underbrace{\begin{bmatrix} b_s + r_s^2 d_{sc} & -r_s^2 d_{sc} & 0 \\ -r_s^2 d_{sc} & b_c + r_s^2 d_{sc} + r_r^2 d_{cr} & -r_r^2 d_{cr} \\ 0 & -r_r^2 d_{cr} & b_r + r_r^2 d_{cr} \end{bmatrix}}_{\tilde{\mathbf{D}}_e} \underbrace{\begin{bmatrix} \omega_s \\ \omega_c \\ \omega_r \end{bmatrix}}_{\tilde{\mathbf{u}}} \tag{4}$$

Figure 8. State space equations of the planetary gear elastic model when $J_s = J_c = J_r = 0$ and the velocities are the inputs.

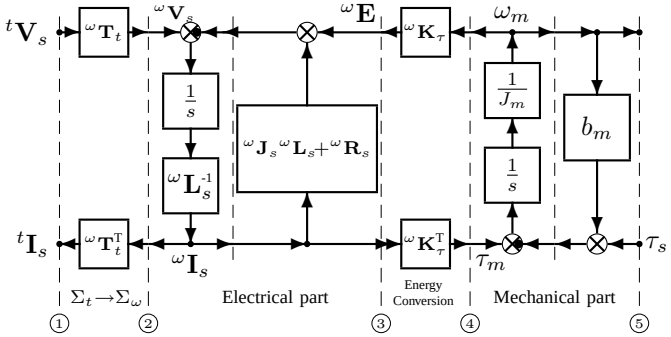

Figure 9. POG scheme of a multi-phase electrical motor in the transformed space Σ_ω.

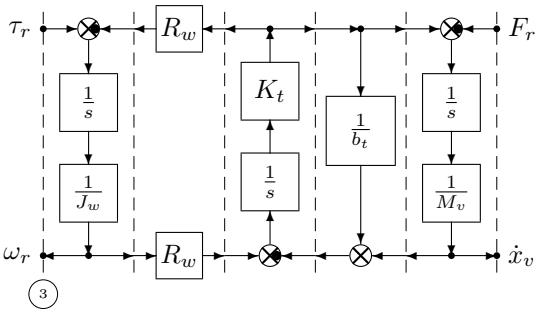

Figure 10. POG scheme of the simplified vehicle model.

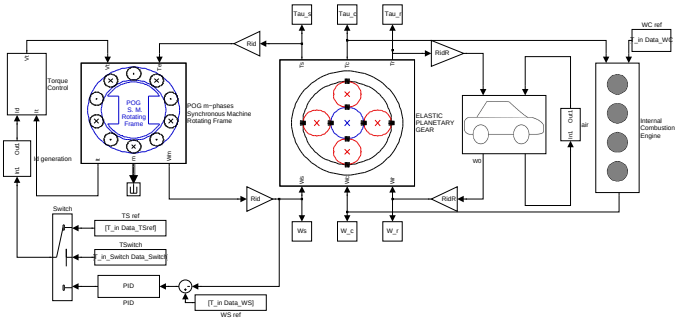

Figure 11. Simulink block scheme of the considered hybrid power structure.

where I_{dk}, I_{qk}, V_{dk} and V_{qk} are, respectively, the *direct* and *quadrature* components of the current and voltage vectors ${}^{\omega}\mathbf{I}_s$ and ${}^{\omega}\mathbf{V}_s$. Note that using transformation ${}^{t}\dot{\mathbf{q}} = {}^{\omega}\mathbf{T}_t^{\mathrm{T}}\,{}^{\omega}\dot{\mathbf{q}}$, the original state space Σ_t has been transformed into $(m_s-1)/2$ two-dimensional orthogonal subspaces named $\Sigma_{\omega k}$ with $k \in \{1:2:m_s-2\}$. A detailed discussion of the properties of vector ${}^{\omega}\mathbf{K}_\tau(\theta)$ can be found in [5].

The POG block scheme of the synchronous motor in the transformed space Σ_ω, see eq. (9), is shown in Fig. 9.

The torque control of the PMSM is realized by the the following control law:

$${}^{\omega}\mathbf{V}_s = ({}^{\omega}\mathbf{R}_s + {}^{\omega}\mathbf{J}_s\,{}^{\omega}\mathbf{L}_s)\,{}^{\omega}\mathbf{I}_s + {}^{\omega}\mathbf{K}_\tau\,\omega_m - \mathbf{K}_c({}^{\omega}\mathbf{I}_s - {}^{\omega}\mathbf{I}_d) \tag{10}$$

where ${}^{\omega}\mathbf{I}_d$ is the constant desired current and $\mathbf{K}_c > 0$ is a diagonal matrix used for the tuning of the control, see [6].

D. Simplified model of the vehicle with tire elasticity

A simplified dynamic model of the vehicle is considered which takes into account also the tire elasticity. The POG scheme is shown in Fig. 10 where J_w is the wheel inertia, R_w is the wheel radius, K_t is the tire longitudinal stiffness, b_t is the friction coefficient and M_v is the mass of the vehicle.

IV. Simulation of the Hybrid Power Structure

The hybrid automotive system shown in Fig. 3-4 has been implemented in Matlab/Simulink as shown in Fig. 11 where the main subsystems are included in masked blocks. In particular, the considered model of the ICE presented in Section III-A has been implemented in Simulink as shown in Fig.12.

Note that the ICE Simulink scheme clearly corresponds to the POG scheme of Fig. 5.

In the considered power-split HEV system many different operation modes are possible, see [8] and [9]: each operation mode corresponds to a different way of controlling the power

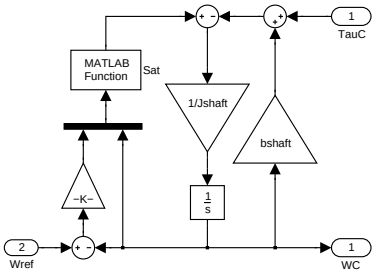

Figure 12. Simulink block scheme of the Internal Combustion Engine model.

	Time [s]	*Operation*
1	0 - 2.5	engine starts while wheels are stopped
2	2.5 - 11	the wheels are released and the vehicle accelerates
3	11 - 12	the vehicle speed is kept constant

Table II
MAIN STEPS IN THE SIMULATION.

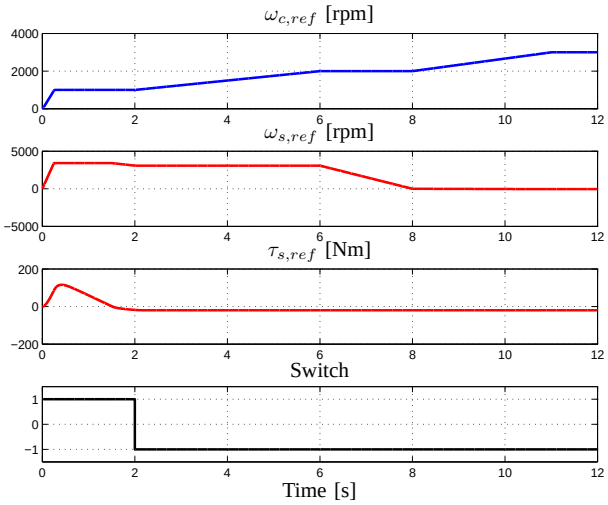

Figure 13. Reference control signals.

flows among the two energy sources and the traction load, remembering that the electrical machine PMSM is a bidirectional power source. In the presented simulations the control of PMSM is either a torque control, see relation (10), or a speed control realized by a PID controller. The *Switch* in the Simulink scheme of Fig. 11 allows to activate either the torque ($S = 1$) or the speed ($S = -1$) control according to the control strategy. The simulation results shown from Fig. 13 to Fig. 17 correspond to three different operating modes: 1) starting of the ICE while wheels are stopped, 2) acceleration of the vehicle, 3) cruise speed of the vehicle. The three operating modes are resumed in Table II. The reference signals $\omega_{c,ref}$, $\omega_{s,ref}$ and $\tau_{r,ref}$ for the carrier velocity ω_c, the sun velocity ω_s and the motor torque τ_s are shown in the upper part of Fig. 13. The switch signal S is shown at the bottom of Fig. 13. The main parameters of the system are reported in Table III. The parameters of the PID controller are: $K_p = 96.9$, $T_i = 4.854$ and $T_d = 0.357$.

The simulation begins with a torque control ($S = 1$) on the PMSM which makes the ICE start. For $t \in [1.6,\ 2]$ s a small negative torque is required in order to have a power flow towards the battery which can be used to recharge the battery. During this phase the vehicle wheels are kept stopped. At $t = 2$ s the speed control of PMSM is activated ($S = -1$) and then at $t = 2.5$ s the wheels are released. For $t \in [2.5,\ 11]$ s the vehicle accelerates from 0 to 130 km/h. The vehicle acceleration is determined by the shape of the speed reference signals $\omega_{c,ref}$ and $\omega_{s,ref}$. At $t = 11$ s the cruise speed is reached. The velocity $\dot{x}_v$ of the vehicle is shown in the upper part of Fig. 14. In the lower part of the same figure the ring

Vehicle			
mass	M_v	1232	kg
wheels moment of inertia	J_w	1.06	kg m^2
wheels radius	R_w	32.55	cm
tires longitudinal stiffness	K_t	3600000	N/m
Planetary Gear			
sun radius	r_s	10.2	cm
ring radius	r_r	24.8	cm
stiffness coefficients	K_{sc}, K_{cr}	10^7	N/m
damping coefficients	d_{sc}, d_{cr}	15000	N s/m
planets moment of inertia	J_p	0.0812	kg m^2
friction coefficients	b_p, b_s, b_c, b_r	0	N m s/rad
Electric motor			
number of phases	m_s	5	
resistance	R_s	0.1	Ω
self induction	L_s	0.03	H
mutual induction	M_{s0}	0.008	H
maximum of the flux function	φ_c	0.9	Wb
moment of inertia	J_m	0.00128	kg m^2
friction coefficient	b_m	0.01	N m s/rad

Table III
MAIN PARAMETERS USED IN THE SIMULATION.

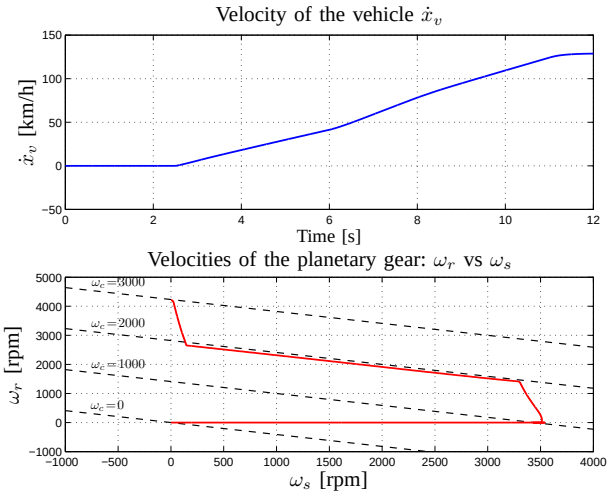

Figure 14. Velocity of the vehicle $\dot{x}_v$ and velocities of the planetary gear: ω_r vs ω_s. The black dashed lines represent lines with constant speed ω_c.

velocity ω_r of the planetary gear is plotted as a function of the sun velocity ω_s, together with some lines at constant carrier velocity ω_c. The velocities ω_s, ω_c, ω_r and the torques τ_s, τ_c, τ_r of the planetary gear are shown in Fig. 15. The power flows within the system are shown in Fig. 16: the power P_b entering the PMSM system is reported in the upper part of the figure, while in the lower part the powers P_s, P_c and P_r at the planetary gear ports are shown. The positive directions of the powers P_b, P_s, P_c and P_r are shown in Fig. 3. In Fig. 17 the torque τ_e provided by the ICE is plotted as a function of the engine speed ω_c together with the maximum engine torque.

Note that with the considered power-split architecture it is not possible to make a strong regenerative braking by controlling the electric motor because the ICE cannot provide negative torques. In fact, at high speed, the electric motor can apply a strong negative torque to the vehicle only in not-regenerative mode. Moreover in this situation the velocities ω_c

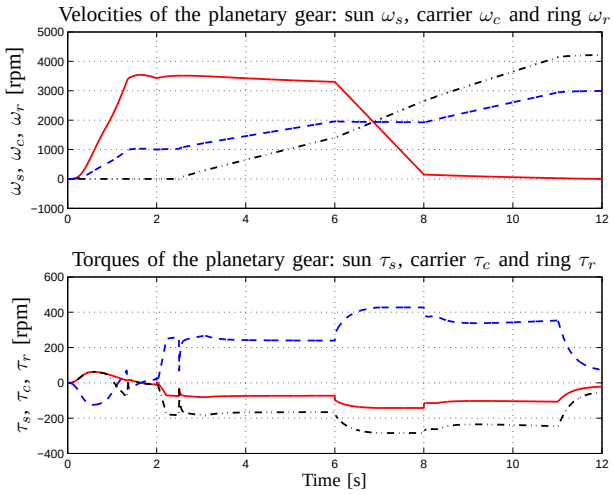

Figure 15. Velocities and torques of the planetary gear: ω_s, τ_s (red, solid), ω_c, τ_c (blue, dashed) and ω_r, τ_r (black, dash-dotted).

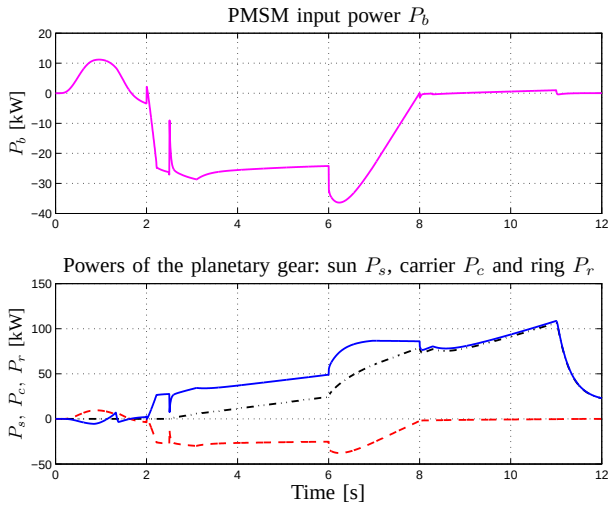

Figure 16. Power flows P_b, P_s, P_c and P_r within the system.

and ω_s of the ICE and the PMSM rapidly reach unacceptable values as shown in the simulation results reported in Fig. 18. The considered power-split architecture allows to make regenerative braking only in the pure electric mode when the ICE is switched off, see [7]. Otherwise, the regenerative braking of the system could be achieved, for example, by adding a second electric machine on the Ring (see the Toyota Hybrid System in [4]) and controlling it properly during braking.

V. Conclusions

In this paper a power-split hybrid electric vehicle is modeled using the Power-Oriented Graphs technique. The model includes a multi-phase permanent magnet synchronous machine, an internal combustion engine, a planetary gear and the vehicle dynamics. The modeled system has been controlled in different operating modes such as engine start, hybrid traction and hybrid braking. Simulation results are provided showing the effectiveness of the proposed model and control.

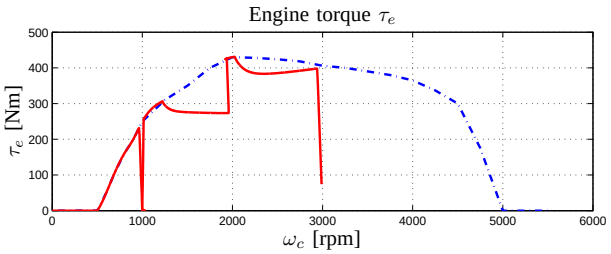

Figure 17. Torque τ_e provided by the ICE versus velocity ω_c.

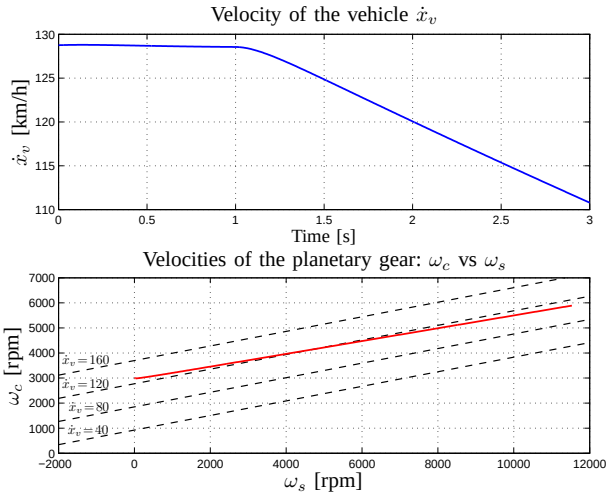

Figure 18. Velocity of the vehicle $\dot{x}_v$ and velocities of the planetary gear: ω_c vs ω_s. The black dashed lines represent lines with constant speed ω_r.

References

[1] R. Zanasi, "Power Oriented Modelling of Dynamical System for Simulation", IMACS Symp. on Modelling and Control of Technological System, Lille, France, May 1991.

[2] Paynter, H.M., *Analysis and Design of Engineering Systems*, MIT-press, Camb., MA, 1961.

[3] D. C. Karnopp, D.L. Margolis, R. C. Rosemberg, *System dynamics - Modeling and Simulation of Mechatronic Systems*, Wiley Interscience, ISBN 0-471-33301-8, 3rd ed. 2000.

[4] Miller, J.M., "Hybrid Electric Vehicle Propulsion System Architectures of the e-CVT Type, IEEE Transactions On Power Electronics, Vol. 21, No. 3, May 2006.

[5] R. Zanasi, F. Grossi "Optimal Rotor Flux Shape for Multi-phase Permanent Magnet Synchronous Motors", International Power Electronics and Motion Control Conference, September 1-3 2008, Poznan, Poland.

[6] R. Zanasi, F. Grossi, "Vectorial Control of Multi-phase Synchronous Motors using POG Approach", IECON 2009, 35th Annual Conference of the IEEE Industrial Electronics Society, November 3-5, 2009 Porto, Portugal.

[7] R. Zanasi, F. Grossi "The POG Technique for Modeling Planetary Gears and Hybrid Automotive Systems" Vehicular Power and Propulsion Conference VPPC 2009, Dearborn, Michigan, USA 7-11 september 2009

[8] K. Chen, W. Lhomme, A. Bouscayrol, A. Berthon "Comparison of two series-parallel Hybrid Electric Vehicles focusing on control structures and operation modes" Vehicular Power and Propulsion Conference VPPC 2009, Dearborn, Michigan, USA 7-11 september 2009

[9] Wenyong Li; A. Abel, K. Todtermuschke,Tong Zhang "Hybrid Vehicle Power Transmission Modeling and Simulation with SimulationX" International Conference on Mechatronics and Automation, ICMA 2007.

[10] Y. Wang, M. Cheng, K.T. Chau, "Review of Electronic - continuously Variable Transmission Propulsion System for Full Hybrid Electric Vehicles", Journal of Asian Electric Vehicles, Vol.2, No.2, 1297-1302, 2009